Wind and Structures, *Vol. 19, No. 1 (2014) 1-14*
DOI: http://dx.doi.org/10.12989/was.2014.19.1.001

Braking performance of working rail-mounted cranes under wind load

Hui Jin* and Da Chen

Jiangsu Key Laboratory of Engineering Mechanics & Key Laboratory of Concrete and Prestressed Concrete Structures of Ministy of Education, Southeast University, Nanjing, 210096, China

(Received August 23, 2013, Revised February 3, 2014, Accepted February 6, 2014)

Abstract. Rail-mounted cranes can be easily damaged by a sudden gust of wind while working at a running speed, due to the large mass and high barycenter positions. In current designs, working rail-mounted cranes mainly depend on wheel braking torques to resist large wind load. Regular brakes, however, cannot satisfactorily stop the crane, which induces safety issues of cranes and hence leads to frequent crane accidents, especially in sudden gusts of wind. Therefore, it is necessary and important to study the braking performance of working rail mounted cranes under wind load. In this study, a simplified mechanical model was built to simulate the working rail mounted gantry crane, and dynamic analysis of the model was carried out to deduce braking performance equations that reflect the qualitative relations among braking time, braking distance, wind load, and braking torque. It was shown that, under constant braking torque, there existed inflection points on the curves of braking time and distance versus windforce. Both the braking time and the distance increased sharply when wind load exceeded the inflection point value, referred to as the threshold windforce. The braking performance of a 300 ton shipbuilding gantry crane was modeled and analyzed using multibody dynamics software ADAMS. The simulation results were fitted by quadratic curves to show the changes of braking time and distance versus windforce under various mount of braking torques. The threshold windforce could be obtained theoretically by taking derivative of fitted curves. Based on the fitted functional relationship between threshold windforce and braking torque, theoretical basis are provided to ensure a safe and rational design for crane wind-resistant braking systems.

Keywords: rail mounted crane; dynamic analysis; braking performace; ADAMS; wind-resistant design

1. Introduction

Nowadays rail mounted cranes are widely used in open areas such as ports, where typhoons or sudden wind gusts are quite common (Fig. 1). Cranes can be easily damaged or even collapse under large wind load while working outside at a running speed, due to their large mass and high barycenter positions as shown in Fig. 2 (Simiu and Scanlan 1986, Forristall 1988, Ochi and Shin 1988, Mara and Asce 2010, Han and Han 2011). The regular brakes cannot stop the crane satisfactorily and ensure its safety in sudden high wind gusts. Therefore, verifications of their braking capacity and a wind-resistant braking design are indispensable for a rail-mounted crane (McCarthy *et al*. 2007, Wu 2011).

*Corresponding author, Associate Professor, E-mail: jinhui@seu.edu.cn

http://www.techno-press.org/?journal=was&subpage=8 ISSN: 1226-6116 (Print), 1598-6225 (Online)

Fig. 1 Rail mounted gantry crane

Fig. 2 Wind crane collapse

Currently, the most commonly used windproof devices for rail mounted cranes include slipper brakes, anchoring devices, brake calipers, etc. Slipper brakes function by pushing the crane under the wheels to avoid slipping (Figs. 3(a) and 3(b)) while anchoring devices by fixing the crane on the ground (Figs. 4(a) and 4(b)). Both types of devices can only be used when the crane is stopped. Brake calipers can be used when the crane is under working conditions, but the brake forces are limited and are not required to be installed strictly (Fig. 5). Despite all these auxiliary devices, the cranes mainly depend on wheel brakes (Fig. 6) to resist large wind load.

(a)

(b)

Fig. 3 Slipper brakes

(a)

(b)

Fig. 4 Anchoring devices

Fig. 5 Brake caliper

Fig. 6 Crane wheel brake

According to the crane design specifications (Zhang *et al*. 2001) , the wheel braking torque should be large enough to keep braking time and distance as short as possible in order to effectively avoid collisions. Since the wheel brakes are also used in normal working conditions, in practice, operators tend to adjust the brakes and reduce the braking torque to avoid the impact and rocking brought in daily use. This adjustment greatly degrades the crane windproof capacity. Reduced braking torque will result in increased braking time and distance, which definitely induces great hidden dangers to the working safety As for these affairs, however, neither preventive measures, nor qualitative or quantitative relations among wind loads, braking torque and braking performance can be refered to.

The braking performance and safety verifications of cranes have been considered as important research topics ever since. Zhang calculated the wind-resistant capacity of cranes through simple theoretical analysis along the railway (Zhang *et al*. 2001). Xu analysed the calculation method of work mechanical parameters and the selection of brakes (Zhang *et al*. 2001). Wu simulated the braking performance of working rail mounted cranes under different types of wind (Wu 2011). Lee analysed the effects of wind loads on the stability of a 50-ton container crane using wind tunnel testing (Lee *et al*. 2007). McCarthy provided recommendations for braking systems (McCarthy *et al*. 2007). But the method to assess the wind-resistant capacity of cranes has not been available in any research report so far. Therefore, there is an urgent need to conduct research works on this topic.

A simplified mechanical model was developed in this work to study working rail mounted cranes with variables like braking time, braking distance, windforce and braking torque. Dynamic analysis of the crane body and wheels based on d'Alembert principle was carried out to deduce braking performance equations which indicate the qualitative relations among these variables. Analysis of results indicated that, when braking torque is a constant, there existed inflection points on the curves of braking time and distance versus windforce. Braking time and distance both increase sharply when wind load exceeds the inflection point value, referred as the threshold windforce.

Furthermore, by simulating a working 300 ton shipbuilding gantry crane using ADAMS, quantitative relations among the study variables are analysed through fitting calculations. With the the obtained quantitative relations, it is easy to determine the threshold windforce under a certain braking torque, which enables scientific evaluations of windproof performance for working cranes.

2. Theoretical analysis

2.1 Simplified mechanical model

A Simplified mechanical model of a typical working rail mounted crane was developed as shown in Figs. 7(a) and 7(b), with a cuboid body, four round wheels and two cylindrical axles.

Dynamic analysis of the crane body and wheels was carried out based on d'Alembert principle considering the equilibrium between inertia force and applied force (see Figs. 8(a) and 8(b)). The wind load is simplified as a constant concentrated force (windforce) applied on the barycenter of the crane body. It is assumed that four wheels are all homogeneous under identical braking torque. As force analyses of four wheels are similar, only the typical analysis process of wheel A is illustrated.

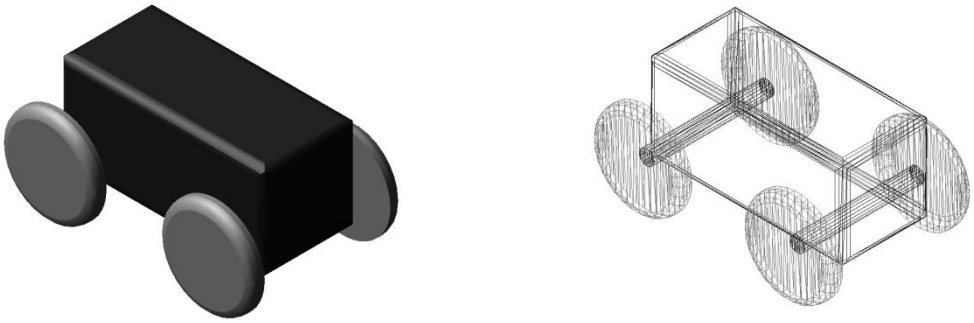

(a) Stereogram (b) Scenograph

Fig. 7 Simplified mechanical model of working rail mounted cranes

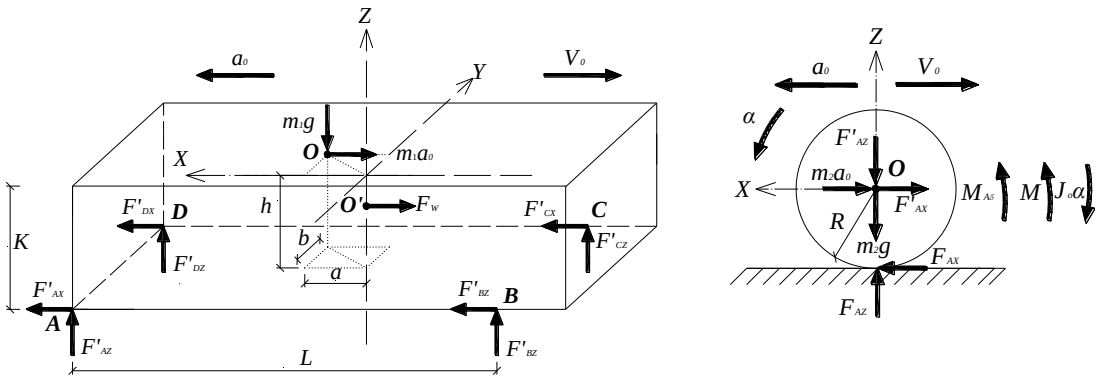

(a) Analysis of the crane body (b) Analysis of wheel A

Fig. 8 Dynamic analysis of the crane body and wheel A

As shown in Fig. 8(a), *X* and *Y* axis are built in the same plane with the barycenter *O* of crane body and *Z* axis passes the centroid *O'*. The initial velocity V_O of crane body is assumed to be along the negative direction of *X* axis, while the braking acceleration a_o is along the positive direction. Equilibrium equations of this spatial force system can be described as

$$\begin{cases} \sum F_X = 0 = F'_{AX} + F'_{BX} + F'_{CX} + F'_{DX} - F_W - m_1 a_0 \\ \sum F_Y = 0 = F'_{AZ} + F'_{BZ} + F'_{CZ} + F'_{DZ} - m_1 g \\ \sum M_{A\text{-}D} = 0 = F'_{CZ} L + F'_{BZ} L - m_1 g(\frac{L}{2} - a) - F_W \frac{K}{2} - m_1 a_0 h \\ \sum M_{C\text{-}D} = 0 = F'_{AZ} K + F'_{BZ} K - m_1 g(\frac{K}{2} - b) = 0 \\ \sum M_Z = 0 = (F'_{AX} - F'_{DX})\frac{K}{2} + (F'_{BX} - F'_{CX})\frac{K}{2} - m_1 a_0 b \end{cases} \tag{1}$$

where $\sum F_X$ and $\sum F_Y$ are the resultant force along *X* and *Y* axis; $\sum M_{A\text{-}D}$, $\sum M_{C\text{-}D}$ and $\sum M_Z$ are the resultant moment around *A-D*, *C-D* and *Z* axis; m_1 specifies the mass of crane body and F_w specifies the windforce applied on the barycenter which shares the same direction with initial velocity; $m_1 a_0$ is the inertia force applied along the opposite direction of *X* axis as well as on the barycenter of crane body. There is no torque from the wheels with axles to connect, only concentrated force along *X* and *Z* axis (F'_{AX}, F'_{BX}, F'_{CX}, F'_{DX} and F'_{AZ}, F'_{BZ}, F'_{CZ}, F'_{DZ}). It is noted that the model ignores the force along *Y* axis. *L* is the distance between two axles and *K* is the height of crane body. *b*, *a*, *h* specify the distances between barycenter *O* and *X* axis, *Y* axis , the bottom surface, respectively.

To analyze the motion of crane wheels, a typical model of wheel A is created as shown in Fig. 8(b), considering the equilibrium of the coplanar force system. The origin of coordinate axis is set at the barycenter *O* of wheel A. All wheels are assumed to be homogeneous with barycenter and centroid being the same point. The motion is assumed to be pure rolling which shares the same velocity and acceleration with the crane body. Equilibrium equations can be described as follows. Eqs. (3) and (4) are the supplementary equations.

$$\begin{cases} \sum F_X = 0 = m_2 a_0 + F'_{AX} - F_{AX} \\ \sum F_Z = 0 = F'_{AZ} + m_2 g - F_{AZ} \\ \sum M_O = 0 = F_{AX} R - M_{A\delta} - M + J_o \alpha \\ M_{A\delta} = \delta F_{AZ} \end{cases} \tag{2}$$

$$a_0 = R\alpha \tag{3}$$

$$J_o = \frac{1}{2} m_2 R^2 \tag{4}$$

In the same manner, $\sum F_X$ and $\sum F_Y$ are the resultant force along *X* and *Y* axis; $\sum M_o$ is the resultant moment around barycenter *O*; m_2 specifies the mass of wheel and *R* specifies the radius; δ means the coefficient of rolling resistance; J_o is the moment of interia. The wheel is assumed to roll under no wind load due to its small volume and low height of the centroid. *M*, $M_{A\delta}$ are the

braking torque and moment of rolling resistance couple which both share the opposite rolling direction with the wheel. While $J_o\alpha$ (the inertia moment applied on the barycenter) shares the same rolling direction with the wheel, but the opposite direction with angular acceleration α. m_2a_0 is the inertia force applied along the opposite direction of acceleration a_0. F_{AX} means the friction force applied from the ground to the wheel with the same direction of acceleration. F_{AZ} specifies the vertical force transferred to the wheel.

All the equilibrium equations deduced from force systems of the crane body and four wheels can be combined together, including 23 equations in total. However, there are a total of 24 unknown parameters in the whole force system, meaning that equations can only be solved with supplementary conditions. Noted that the relations between acceleration a_0, windforce F_W and braking torque M can be deduced from variable substitution of these equations, as shown in Eq. (5); the braking performance equations (equations of braking time t and distance s) are shown in Eqs. (6) and (7). The qualitative relations, indicated from the braking performance equations, can be used to analyse the influence from wind load and braking torque on braking time and distance.

$$a_0 = \frac{-F_W R + \delta(m_1+4m_2)g + 4M}{(m_1 + 6m_2)R} \tag{5}$$

$$t = \frac{V_0(m_1 + 6m_2)R}{4M - F_W R + \delta(m_1 + 4m_2)g} \tag{6}$$

$$s = \frac{V_0^2(m_1 + 6m_2)R}{2[4M - F_W R + \delta(m_1 + 4m_2)g]} \tag{7}$$

2.2 Results and discussion

The relevant data of a 40 ton gantry crane are substituted into Eqs. (6) and (7) to obtain curves of braking time and distance versus windforce under constant braking torque, as shown in Figs. 9(a) and 9(b).

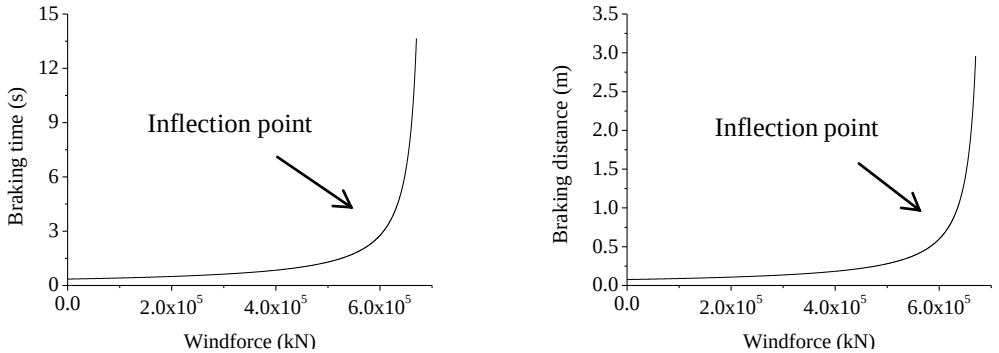

(a) Curves of braking time (b) Curves of braking distance

Fig. 9 Curves of braking time and distance versus windforce under a certain constant braking torque

Observed from the above figures, inflection points clearly exist on the curves of braking time and distance versus windforce. Braking time and distance both sharply increase when wind load exceeds the inflection point value, e.g., the threshold windforce.

The safety of working cranes can be evaluated based on the threshold windforce which has a one-to-one relation with braking torque. When the wind load is smaller than threshold windforce, a small change of wind load will not result in large changes of braking time and distance. As the safety foundation of working rail mounted cranes, developing the relations between braking torque and threshold windforce can provide theoretical basis to calculate the reasonable braking torque, which ensures that the corresponding threshold windforce is larger than the practical wind load.

3. Numerical simulation

Gantry crane is one kind of the most commonly used large cranes in shipbuilding. Through dynamic analysis using software ADAMS, a 300t shipbuilding gantry crane is taken as the research object to study the relation between braking torque and threshold windforce.

The overall structural dynamic performance under the combination effect of braking torque and wind load is the key issue in this research, so the structural internal force is ignored and the entire crane superstructure is simplified as a rigid body connected with 64 crane wheels. The number of brake wheels, which are intervally arranged, is 32, accounting for half of the total number of wheels. The finite element model in ADAMS/View displays in Figs. 10(a) and 10(b).

The railway tracks are built directly on the ground as a whole without any contact settings. Revolution joints are used to connect wheels to the axles, while other parts of the crane are assembled into an integral body through Boolean operation. Coulomb contact force is applied wherever wheels and the railway tracks contact, following the *IMPACT* function (Fan *et al*. 2006, Yu and Qian 2006) as shown by Eq. (8).

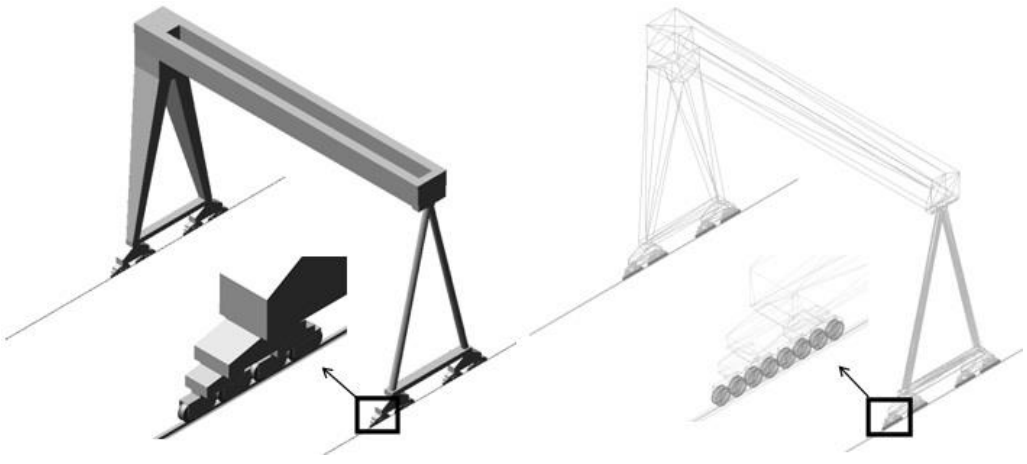

(a) Stereogram (b) Scenograph

Fig. 10 Model of 300t shipbuilding gantry crane

$$IMPACT = \begin{cases} Max(\,0,\, k\,(\,x_1\text{-}x)^e - \ STEP(\,x,\, x_1 - d,\, c_{max},\, x_{1,}\, 0) \cdot \dot{x} & x < x_1 \\ 0 & x \geq x_1 \end{cases} \tag{8}$$

where x specifies a distance variable that is used to compute the *IMPACT* function; x_1 is a positive real variable that specifies the free length of x; $\dot{x}$ specifies the time derivative of x to *IMPACT*; k is a non-negative real variable that specifies the stiffness of the boundary surface interaction; e is a positive real variable that specifies the exponent of the force deformation characteristic; c_{max} means a non-negative real variable that specifies the maximum damping coefficient; d is a Positive real variable that specifies the boundary penetration at which Adams/Solver (C++) applies full damping; *STEP* approximates a step function with a cubic polynomial which can be defined as follows

$$STEP(x,\, x_0,\, h_0,\, x_1,\, h_1) = \begin{cases} h_0 & x \leq x_0 \\ h_0 + (\,h_1 - h_0)[(x - x_0)/(x_1 - x_0)]^2\{3 - 2[(x - x_0)/(x_1 - x_0)]\} & x_0 < x < x_1 \\ h_1 & x \geq x_1 \end{cases} \tag{9}$$

The wind load is simplified as a constant concentrated force applied on the barycenter of crane body, as shown in Fig. 11. Braking torque is applied on the revolution joints of the brake wheels (see Fig. 12). Simultaneously, moment of rolling resistance couple is imposed on every revolution joint.

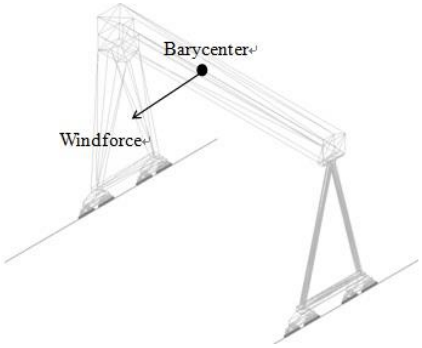

Fig. 11 Windforce on crane

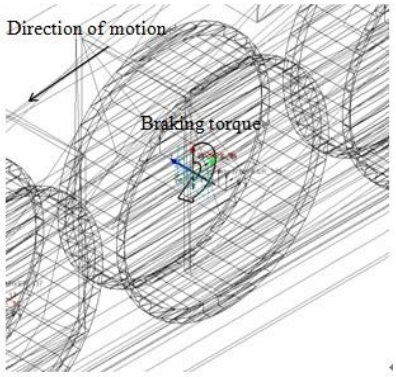

Fig. 12 Braking torque on brake wheel

The model above is employed to simulate the braking performance of a 300 ton shipbuliding gantry cranes under different working conditions, which include various delay time (time between the application of windforce and the working of braking torque), initial velocities, wind loads, etc. The simulation results reveal the relations between braking torque and threshold windforce.

4. Results and discussion

4.1 Numerical simulation results

The typical working condition is described as follows. The windforce applied on the crane is 752.06 kN (fresh gale) and the initial velocity is 0.6 m/s with the same direction as the windforce. Delay time is set to be 1s. The braking torque, which is adjusted on the basis of the wind load, is 10 kN·m according to the above working conditions. Curves of velocity and distance versus time can be obtained from the simulation of ADAMS, as shown in Figs. 13(a) and 13(b) which illustrates the braking time (t = 11.40 s) and according braking distance (s = 4.85 m). Vibrations are found in the progress of crane's motion along the railway tracks, which can be explained by the vibrations of contact force and torque between the wheels and tracks with gradually reducing amplitudes (see Figs. 14(a) and 14(b)).

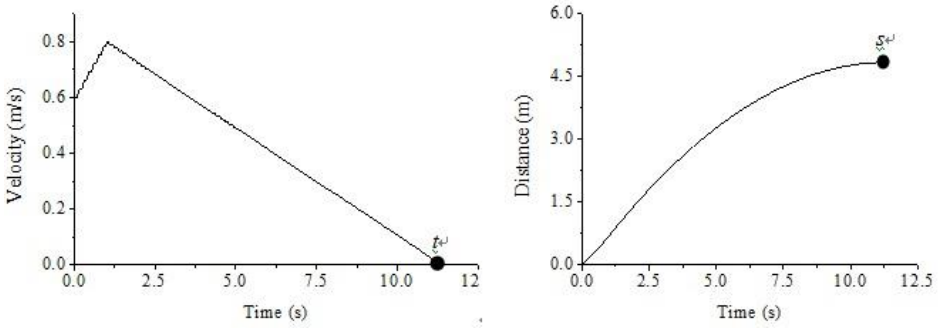

(a) Curve of velocity (b) Curve of distance

Fig. 13 Curves of velocity and distance versus time

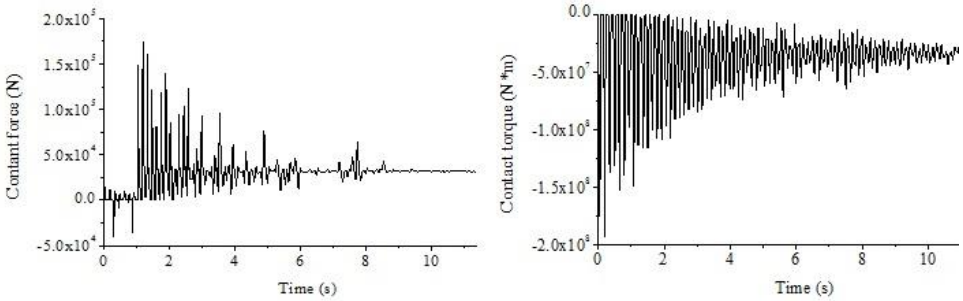

(a) Curve of contact force (b) Curve of contact torque

Fig. 14 Curves of wheel contact force and torque versus time

Table 1 Change rates of braking time and distance

	Windforce 752.1kN		Windforce 561.8kN		Change rate	
	Braking Time(s)	Distance (m)	Braking Time(s)	Distance (m)	T (%)	S (%)
Delay time (s)	Initial velocity 0.6m/s					
0	7.6	2.2943	4.5	1.371	40.79	40.24
1	11.4	4.8469	6.75	2.8272	40.79	41.67
2	15.1	8.1784	8.95	4.6294	40.73	43.39
3	18.8	12.2762	11.15	6.769	40.69	45.59
Initial velocity (m/s)	Delay time 1s					
0.45	9.45	3.3059	5.6	1.9121	40.74	42.16
0.6	11.4	4.8469	6.75	2.8272	40.79	41.67
0.75	13.3	6.6736	7.9	3.9137	40.6	41.36

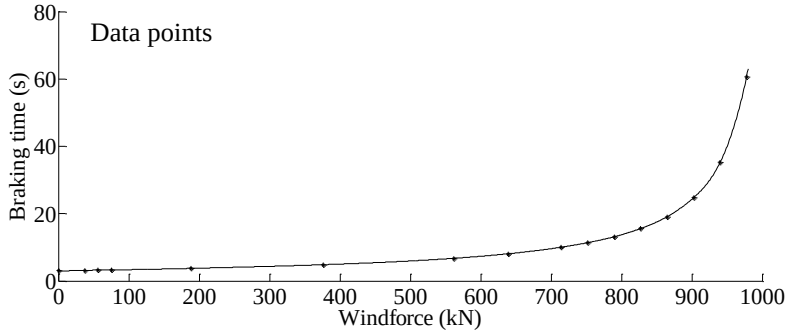

(a) Curve of braking time

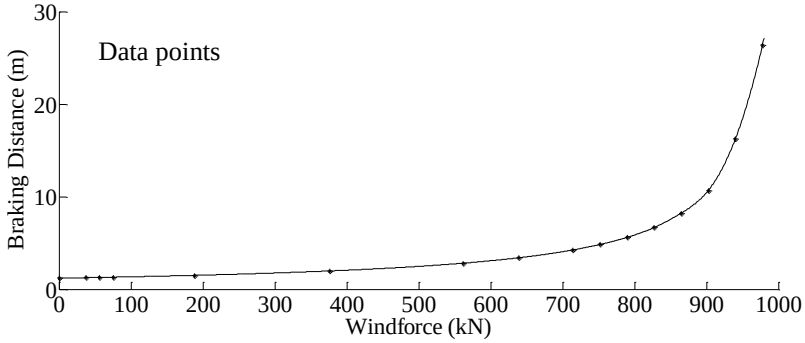

(b) Curve of braking distance

Fig. 15 Curves of braking time and distance under constant braking torque

According to the following simulation results, change rates of braking time and distance are closely related to windforce and braking torque. To eliminate other influence factors, simulations of cranes under different working conditions with constant braking torque $10\,\mathrm{kN{\cdot}m}$ are carried out. The results shown in Table 1 proves that changes of delay time and initial velocity have little

impact on the change rates of braking performance, although different delay time and initial velocities do have a great impact on the specific values of braking time and diatance. This means the change rates of braking time and distance are only relevant to windforce and braking torque. In other words, inflection points, which are the catastrophe points of change rates, will keep the same no matter how delay time and initial velocities change. The threshold windforce, corresponding to the inflection points, is also unrelated to the working conditions except for the braking torque and windforce. Therefore, in order to analyse the relation between braking torque and threshold windforce, only the working condition with typical delay time and initial velocity is simulated, just under various braking torques and windforces.

Based on the typical working condition, braking performance of the 300 ton shipbuilding gantry crane is simulated under different windforce to obtain the function curves of braking time and distance versus windforce under constant braking torque, as shown in Figs. 15(a) and 15(b). Cubic splines interpolation is used to get smooth curves, which show the same characteristics as curves in Fig. 9 from theoretical analysis. This means the threshold windforce exists in all kinds of rail mounted cranes.

The curves of breaking time versus windforce subjected to various braking torque are systematically shown in Figs. 16(a) and 16(b). Corresponding to the inflection points on the curves, the threshold windforce increase significantly with the increasing braking torque. Additionally, the braking time and distace decrease with the increasing braking torque under the same windforce.

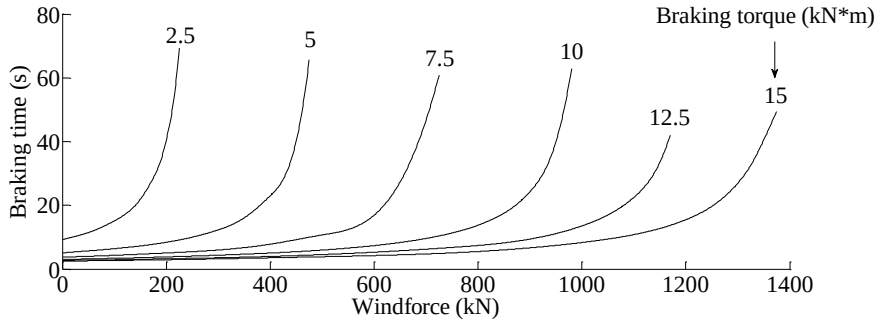

(a) Curve of braking time

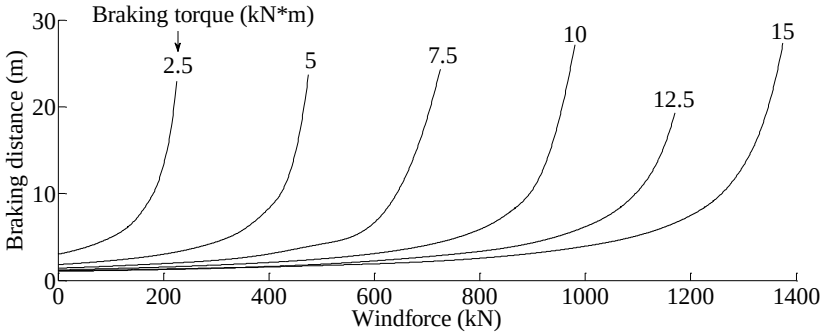

(b) Curve of braking distance

Fig. 16 Curves of braking time and distance under different braking conditions

4.2 Analysis and discussion

As displayed in the figures above, when braking torque remains the same, inflection points that correspond to the threshold windforce will exist on the curves of braking time and distance. However, it is still difficult to determine the accurate threshold windforce for each curve. This is because the changes of braking time and distance are all continuous without definite catastrophe points.

One important characteristics of cubic splines interpolation is that the first order derivative of the interpolation point must be continous. Through derivation of spline interpolation functions gives the curves of derivative functions, which show the change rates of braking time and diatance and can explicitly reveal the mutation process of change rates and the threshold windforce (see Figs. 17(a) and 17(b)).

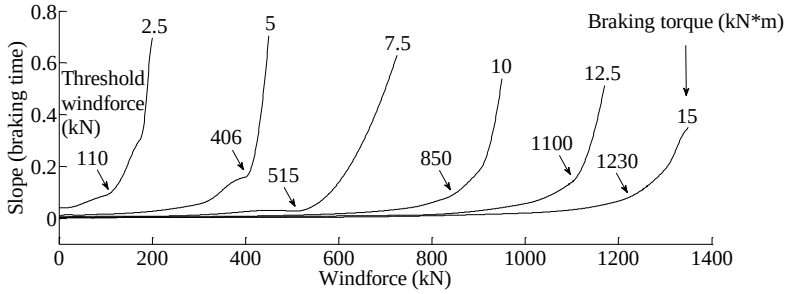

(a) Derivative function curve of braking time

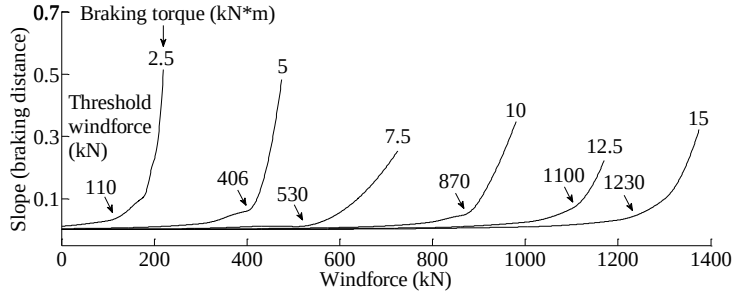

(b) Derivative function curve of braking distance

Fig. 17 Derivative function curves of braking time and distance under different braking conditions

As shown in the figures above, derivative function curves mutate evidently when windforce reaches the threshold value, accompanying with rapid increase of braking time and distance.

Different threshold windforces under different braking torque can be obtained from the catastrophe points on the curves in Figs. 17(a) and 17(b), as shown in Table 2. Threshold windforces deduced from change rate curves of braking time and distance are almost the same, except when the braking torque is 7.5×10^{3}N·m and 1×10^{4}N·m. To ensure the one-to-one relation between threshold windforce and braking torque, average values are used to represent different threshold windforce under different braking torque (see Table 2).

Table 2 Different threshold windforce under different braking torque

Braking torque (kN*m)	2.5	5	7.5	10	1.25	15
Threshold windforce (time) (kN)	110	406	515	850	1110	1230
Threshold windforce (distance) (kN)	110	406	530	870	1110	1230
Averages (kN)	110	406	522.5	860	1110	1230

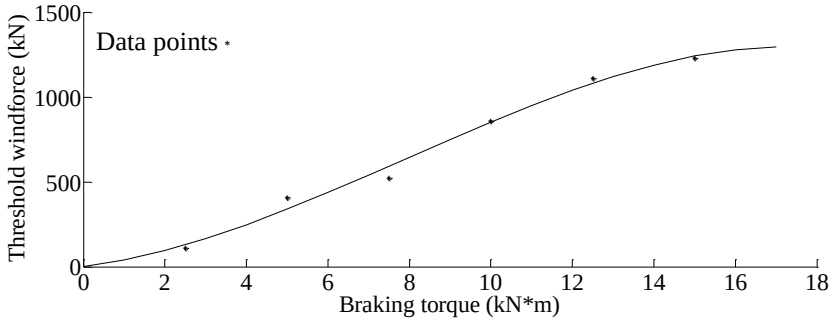

Fig. 18 Function curve of threshold windforce versus braking torque

The function curve of threshold windforce versus braking torque can be obtained from curve fitting analysis of the above data, as shown in Fig. 18. According to the calculation, a cubic curve is identified to be the most suitable curve. Since threshold windforce on fitting curves of orders other than three turn into zero when the braking torque is still positive, which is wrong, only the cubic curve may represent the turth.

The cubic fitting function of threshold windforce F_W versus braking torque M can be described as

$$F_W = -0.4018M^3 + 9.5581M^2 + 29.6921M + 2 \tag{10}$$

The above equation can be used to evaluate the windproof performance of the working 300 ton shipbuilding gantry cranes. With practical braking torque being substituted in this equation, if the calculated threshold windforce is larger than the applied practical windforce, the safety of cranes can be ensured with no great change of braking performance; Else if the calculated threshold windforce is smaller than the applied practical windforce, the crane is under hidden dangers with great change of braking time and distance corresponding to the windforce change. In the last case, it is very easy for braking time and disrance to get too long to avoid collision and hence to cause severe accidents. Keeping threshold windforce, corresponding to the practical braking torque, larger than the practical windforce applied on the working rail mounted cranes is the key point to guarantee the braking performance for wind resistance and to ensure the crane safty.

5. Conclusions

A simplified mechanical model has been developed to analyse the braking performance of

working rail-mounted cranes. In addition, the 300 ton shipbuilding gantry crane is taken as the research object in dynamic analysis by ADAMS to obtain the function curves of braking time and distance versus windforce. Conclusions from this study are summarized as follows:

(1) Under constant braking torques, inflection points exist on the curves of braking time and distance versus windforce. Both braking time and distance increase much more sharply when the wind loads exceed the inflection point force.

(2) The threshold windforce is only related to the braking torque and windforce and will increase significantly with the increase of braking torque.

(3) Different threshold windforces corresponding to different braking torques can be obtained, and their fitting relationship function can be used to evaluate the windproof performance of cranes.

Acknowledgments

The research was supported by the Science and Technology Project of General Administration of Quality Supervision, Inspection and Quarantine of the People's Republic of China (2009QK153, 2009QK149), Jiangsu Province Science and Technology Support Project (BE2012125) and A Project Funded by the Priority Academic Program Development of Jiangsu Higher Education Institutions.

References

Fan, J.C., Xiong, G.M. and Zhou, M.F. (2006), *Application and improvement of virtual prototype software MSC.ADAMS*, China Machine Press, Beijing, China.

Forristall, G.Z. (1988), *Wind spectra and gust factors over water*, OTC 5735, Houston, USA.

Han, D.S. and Han, G.J. (2011), "The difference in the uplift force at each support point of a container crane between FSI analysis and a wind tunnel test", *Mech. Sci. Technol.*, **25**(2), 301-308.

Lee, S.W., Shim, J.J., Han, D.S., Han, G.J. and Lee. K.S. (2007), "An experimental analysis of the effect of wind load on the stability of a container crane", *Mech.Sci. Technol.*, **21**(3), 448-454.

Mara, T.G. and Asce, A.M. (2010), "Effects of a construction tower crane on the wind loading of a high-rise building", *J. Struct. Eng. - ASCE*, **136**(11), 1453-1460.

McCarthy, P., Soderberg, E. and Dix, A. (2009), "Wind damage to dockside cranes: recent failures and recommendations", *Proceedings of the Technical Council on Lifeline Earthquake Engineering Conference (TCLEE) 2009*, Oakland, California, United States, June.

Ochi, M.K. and Shin, Y.S. (1988), *Wind turbulent spectra for design consideration of offshore Structures*, OTC 5735, Houston, USA.

Simiu, E. and Scanlan, R.H. (1986), *Wind effects on structures*, Wiley & Son Inc, Houston, USA.

Wu, X.L. (2011), *Dynamic analysis and application of wind-proof for working rail mounted crane*, MSE. Dissertation, Southeast University, Nanjing, China.

Yu, D.Y. and Qian, Y.J. (2006), "Parameter - settings for the dynamic simulation based on ADAMS", *Comput. Simulation*, **23**(9), 103-183.

Zhang, Z.W., Yu, H.Q., Wang, J.N. and Bao, Q.F. (2001), *Crane design manual*, (2nd Ed.), China Railway Publishing House, Beijing, China.

JH